photonics

MDPI

Review

Rare-Earth-Doped Selenide Glasses as Laser Materials for the 5–6 μm Spectral Range

Boris Denker [1], Peter Fjodorow [2], Mikhail Frolov [3], Boris Galagan [1], Vasily Koltashev [4], Victor Plotnichenko [4], Maxim Sukhanov [5], Sergei Sverchkov [1,*] and Alexander Velmuzhov [5]

1 Prokhorov General Physics Institute of the Russian Academy of Sciences, 119991 Moscow, Russia; denker@lst.gpi.ru (B.D.)
2 Institute for Combustion and Gas Dynamics—Reactive Fluids, University of Duisburg-Essen, 47057 Duisburg, Germany; peter.fjodorow@uni-due.de
3 P.N. Lebedev Physical Institute of the Russian Academy of Sciences, 119991 Moscow, Russia; frolovmp@x4u.lebedev.ru
4 Prokhorov General Physics Institute of the Russian Academy of Sciences, Dianov Fiber Optics Research Center, 119991 Moscow, Russia; victor@fo.gpi.ru (V.P.)
5 Devyatykh Institute of Chemistry of High-Purity Substances of the Russian Academy of Sciences, 603951 Nizhny Novgorod, Russia
* Correspondence: glasser@lst.gpi.ru

Abstract: This paper provides an overview of mid-infrared lasers based on rare-earth-ion-doped selenide glasses. Laser action was demonstrated at the transitions between the first excited and the ground levels of Ce^{3+}, Pr^{3+}, Nd^{3+} and Tb^{3+} ions. The highest output parameters for bulk glass lasers (over 40 mJ of output energy) and wavelength tuning in the range of 4.6–5.6 microns were obtained with Ce^{3+}-doped glass. The highest output parameters for fiber lasers (150 mW at 5.1–5.3 μm under continuous pumping) were demonstrated with Tb^{3+} ions. The longest lasing wavelengths for any glass laser and tunability within the 5.56–6.01 μm spectral band were shown with Nd^{3+} ions in a Tb^{3+}-Nd^{3+} co-doped system.

Keywords: selenide glass; chalcogenide optical fiber; mid-infrared glass laser

Citation: Denker, B.; Fjodorow, P.; Frolov, M.; Galagan, B.; Koltashev, V.; Plotnichenko, V.; Sukhanov, M.; Sverchkov, S.; Velmuzhov, A. Rare-Earth-Doped Selenide Glasses as Laser Materials for the 5–6 μm Spectral Range. *Photonics* **2023**, *10*, 1323. https://doi.org/10.3390/photonics10121323

Received: 16 October 2023
Revised: 21 November 2023
Accepted: 27 November 2023
Published: 29 November 2023

1. Introduction

Various applications require the use of laser radiation from the mid-infrared (MIR) spectral range [1]. The sources of coherent radiation can be divided into two large groups: lasers based on population inversion and wavelength converters based on nonlinear optics. This review is not concerned with nonlinear optical devices and is devoted to newly developed solid-state laser materials emitting within the mid-infrared range. At the present time, broadband-gain media suitable for tunable lasers as well as for ultrashort pulse amplifiers are being actively investigated. Compact solid-state laser systems are of particular interest.

In the 1980s, color-center lasers [2] found widespread use in various applications, especially in spectroscopy. The main drawbacks complicating the usage of these lasers include the instability of the laser-active color centers and the necessity for cryogenic cooling, especially in the mid-infrared spectral region.

Although quantum cascade lasers [3] provide access to a large part of the MIR, their fabrication is still expensive, while the output powers/energies are orders of magnitude below the solid-state lasers' (SSLs') performance.

Significant progress in the development of MIR solid-state lasers has been achieved in crystals based on Fe^{2+}-doped chalcogenide materials [4–8], among which the longest wavelength tuning range of 4.5–6.8 μm was achieved with the Fe^{2+}:CdTe laser. However, the short upper-state lifetimes (in the sub-μs range) and the need for cryogenic cooling make the implementation of these lasers difficult in practice.

Rare-earth-ion-doped short phonon-spectra crystals and glasses have long been considered promising host materials for lasers operating in the mid-infrared range. Their undoubted advantages over Fe^{2+} and color-center lasers are the millisecond lifetimes of the upper laser levels, enabling long pump pulses. The number of papers describing rare-earth-doped crystalline laser materials for wavelengths exceeding 4 μm is rather limited. These lasers are still in their infancy, and their output energies are typically well below 1–2 mJ [9–12].

The main advantage of glasses over crystals is the possibility to draw optical fibers from them. This fiber configuration easily allows efficient cooling that is required for continuous operation and diffraction-limited beam quality. However, until 2020, the longest wavelength emitted by a rare-earth-doped glass laser was 3.92 μm. It was a Ho-doped indium fluoride glass–fiber laser [13]. Further wavelength increases in fluoride laser glasses is prevented by the multiphonon luminescence quenching of rare-earth-ion transitions.

It should also be noted that, in parallel, work is being developed with gas-filled hollow optical fibers, which demonstrate coherent radiation in the mid-infrared range due to either inversion or stimulated Raman scattering [14,15].

This review is devoted to the recently appeared rare-earth-doped chalcogenide glass lasers. Chalcogenide glasses differ from traditional oxide and fluoride ones by their shorter phonon spectrum, resulting in an infrared transparency extending to ~10 μm in sulfides, ~15 μm in selenides and ~20 μm in tellurides. On the other hand, their transparency window opens on the short-wavelength side at ~0.6–0.8 μm for sulfides, ~0.8–1.2 μm for selenides and ~2–3 μm for tellurides. In other words, selenide and telluride glasses are completely opaque in the visible range. Other notable features of chalcogenide glasses are their high refractive indices and high resistance to atmospheric moisture, which are much better than those of zirconium-based fluoride glass, for example.

In contrast to simple As-S and As-Se glasses, multicomponent Ge- and/or Ga-containing chalcogenide glass compositions are capable of dissolving significant amounts of rare-earth ions. The prospects of chalcogenide glasses as materials for bulk and fiber long-wavelength lasers, with $\lambda > 4$ μm, have been recognized for several decades already. Dozens of works have been devoted to the synthesis and investigation of rare-earth-doped chalcogenide glasses. Multiple international research groups from the UK (the University of Nottingham, Nottingham, UK), Poland (Wroclaw University of Technology, Wrocław, Poland), France (the University of Rennes, Rennes, France, the University of Caen Normandy, Caen, France), the USA (Naval Research Laboratory, NASA Langley Research Center and National Institute of Aerospace, Hampton, VA, USA), Australia (Macquarie University, Sydney, Australia), Russia (Prokhorov General Physics Institute, Moscow, Russia, Devyatykh Institute of Chemistry of High-Purity Substances, Nizhny Novgorod, Russia), the Republic of Korea, China and some other groups have thoroughly studied the luminescent properties of rare-earth-doped chalcogenide glasses. The main results of these works are summarized in reviews [16–19]. Nevertheless, attempts to obtain mid-infrared laser action in chalcogenide glasses did not bring success for many years. A considerable number of works appeared with the words "laser" or "source of coherent radiation" in the title (see [18,20–23] for example), but the only positive result for a long time was the observation of a laser effect in the near infrared (at 1.08 μm in Nd^{3+}-doped sulfide glasses) [24].

Now, it has become clear that the absence of the laser effect in the mid-infrared was due to the absorption losses and rare-earth luminescence quenching caused by impurities introduced in the investigated glasses, together with rare-earth elements [25]. The most harmful impurities were hydrogen-containing (Se-H, Ge-H) and oxygen-containing (Ge-O, As-O) groups having characteristic absorption bands in the spectral ranges of 3.7~5.3 μm and 5.3~8 μm, respectively. One more problem was the intensive light scattering by heterogenic inclusions in the glasses.

The situation began to change in 2019–2020 after the first demonstrations of positive on–off gain [26] and an actual lasing effect [27] at about 5 μm in Pr^{3+}- and Tb^{3+}-doped

selenide glasses. At the present time, the obtained lasing wavelengths cover the spectral range from 4.5 to 6 microns. This spectral interval falls, at least partially, within the transparency window of the earth's atmosphere.

2. Preparation of Rare-Earth-Ion-Doped High-Purity Glasses Based on Germanium, Antimony and Gallium Selenides

The main source of impurities in the doped selenide glasses are rare-earth metals and their precursors (halides, chalcogenides). The total optical losses in glasses caused by impurities brought with rare-earth metals at a doping level of 1000 wt ppm can reach 10–85 dB/m [25]. Traditional preparation methods of undoped high-purity glasses based on arsenic, germanium and antimony chalcogenides include the distillation of initial components and charging. This makes it possible to reduce the content of most nonvolatile impurities as well as the content of gas-forming impurities (hydrogen, oxygen) and of heterogeneous inclusions. The difficulty in applying this approach to the preparation of rare-earth-doped glasses and glasses containing gallium is that Ga and rare-earth metals and their chalcogenides are not volatile, even at relatively high temperatures (over 750 °C) and cannot be purified by simple distillation or by distillation after melting with chemical getters that reduce the content of hydrogen and oxygen impurities. As a result, the minimum achieved content of hydrogen impurity in the form of Se-H groups in rare-earth-doped chalcogenide glasses was about 10 ppm [28,29]. This is 1–2 orders of magnitude higher than in undoped glasses. The content of other impurities (heterogeneous inclusions, transition metals) was not analyzed in the literature.

The authors of [30] have developed methods for the preparation of high-purity chalcogenide glasses of the Ge-Se(S), Ge-As-S and Ga-Ge-As-Se systems using germanium loading by chemical distillation of its volatile monochalcogenide and gallium loading by chemical transport reactions. These methods have made it possible to reduce the content of hydrogen impurities in the form of Se-H groups and oxygen in the form of Ge-O groups to a level of 0.01–0.1 ppm. Based on these methods, we have proposed a two-stage procedure for the preparation of rare-earth-doped chalcogenide glasses, in which all the charge components (Ge, Sb, Ga, Se) as well as the rare-earth metals are loaded and additionally purified by a combination of germanium and antimony selenide distillation and the chemical vapor transport of gallium and rare-earth metal iodide under high vacuum conditions. Using this method, high-purity $Ga_5Ge_{20}Sb_{10}Se_{65}$ glasses doped with Ce, Pr, Nd, Tb and Dy were prepared. This composition remains crystallization-stable up to a rare-earth-ion concentration of about 10^{20} cm^{-3}. This is a sufficiently high value, which makes it possible to utilize the processes of nonradiative excitation transfer between active ions and thus to organize complicated (cross-relaxation, sensitization) pumping schemes. An advantage of the developed method is the synthesis and loading of hygroscopic iodides of rare-earth metals under high vacuum conditions, which makes it possible to significantly reduce the content of hydrogen- and oxygen-containing impurities as well as that of heterogeneous inclusions in glasses (Figure 1a).

The total content of transition-metal impurities in the best glass samples was 0.03 wt ppm; that of hydrogen, 0.01 wt ppm; and that of micron-sized heterogeneous inclusions, less than 10^2 cm^{-3}. Figure 1b shows the attenuation spectra of a glass sample with 1.0 wt % of Dy. The usage of Dy^{3+} ions having no absorption overlapping with the Se-H group absorption band (at 4.5 μm) makes it possible to demonstrate the efficiency of the glass purification technique. The mentioned synthesis methods of rare-earth-doped chalcogenide glasses enabled us to obtain reproducible and practically significant output characteristics of mid-infrared bulk and fiber lasers.

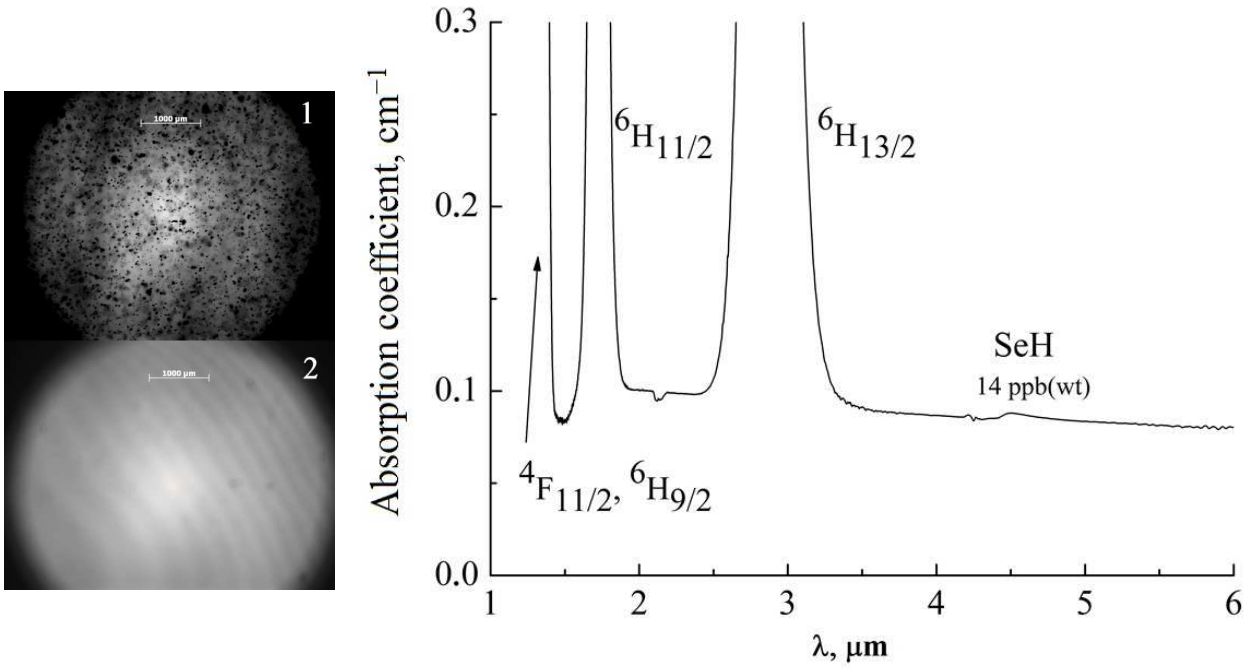

(**a**) (**b**)

Figure 1. (**a**) Overview of optical microscopic images of micron-sized inclusions in rare-earth-doped glasses prepared by the traditional method (1) and by the method (2) described in [30]. (**b**) Attenuation spectrum of $Ga_5Ge_{20}Sb_{10}Se_{65}$ glasses doped with 1.0 wt % of Dy prepared as described in [30].

3. The Choice of Lasing Ions and Transitions

First of all, it makes sense to clarify the spectral range for which the development of selenide laser glasses is reasonable. On the short-wavelength side, there is a restriction for the pump and lasing wavelengths caused by the transparency window of selenide glasses. Apparently, there are no fundamental obstacles to obtaining laser action with wavelengths starting from 1.3 to 1.5 μm in selenide glasses. However, in addition to physical limitations, the competition with already developed laser materials should be taken into account. As already mentioned, well-developed fluoride-based laser glasses and fibers are capable of operating at up to almost 4 μm and, thus, it is less interesting to develop new laser glasses for shorter wavelengths.

In selenide glasses, the luminescence of rare-earth ions could be observed at wavelengths reaching 7–8 μm [31–36], although the characteristic relaxation times of such transitions are limited to microseconds or tens of microseconds and the quantum yield is low or not defined. However, there are a number of rare-earth ions demonstrating intensive 4–6 μm luminescence with high quantum yields and relaxation times in the millisecond range. Thus, the latter spectral range looks the most promising for the development of selenide laser glasses.

Figure 2 shows the energy-level schemes of the four trivalent rare-earth ions that enabled lasing in selenide glasses. The laser transitions are indicated by red arrows and the pump wavelengths by black ones. Note that all these laser transitions have a common feature: all of them are between the first excited and the ground states of the corresponding ion. Such situations are associated with the limited short-wave transparency of selenide glasses: one cannot use high-lying energy levels for either pumping or lasing.

The spectral properties of these laser transitions were analyzed in [37]. The experimentally observed emission cross-section profiles were compared with the cross-sections calculated according to the McCumber formalism. Figure 3 presents the calculated and experimentally stimulated emission cross-sections, and Table 1 shows the calculated radia-

tive and experimentally measured luminescent lifetimes of the above-mentioned rare-earth transitions in selenide glasses.

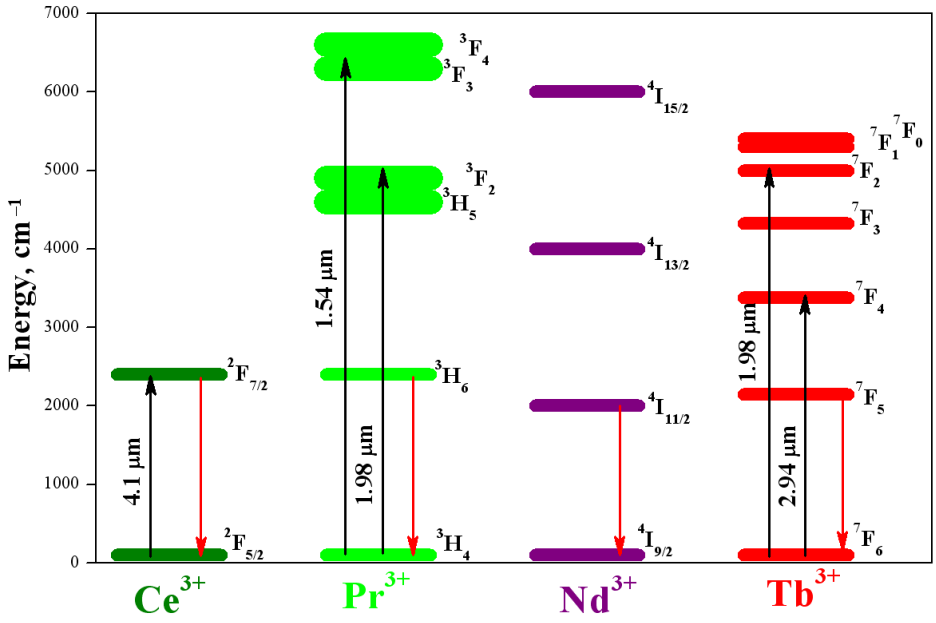

Figure 2. Pumping and lasing transitions of rare-earth ions in selenide glasses.

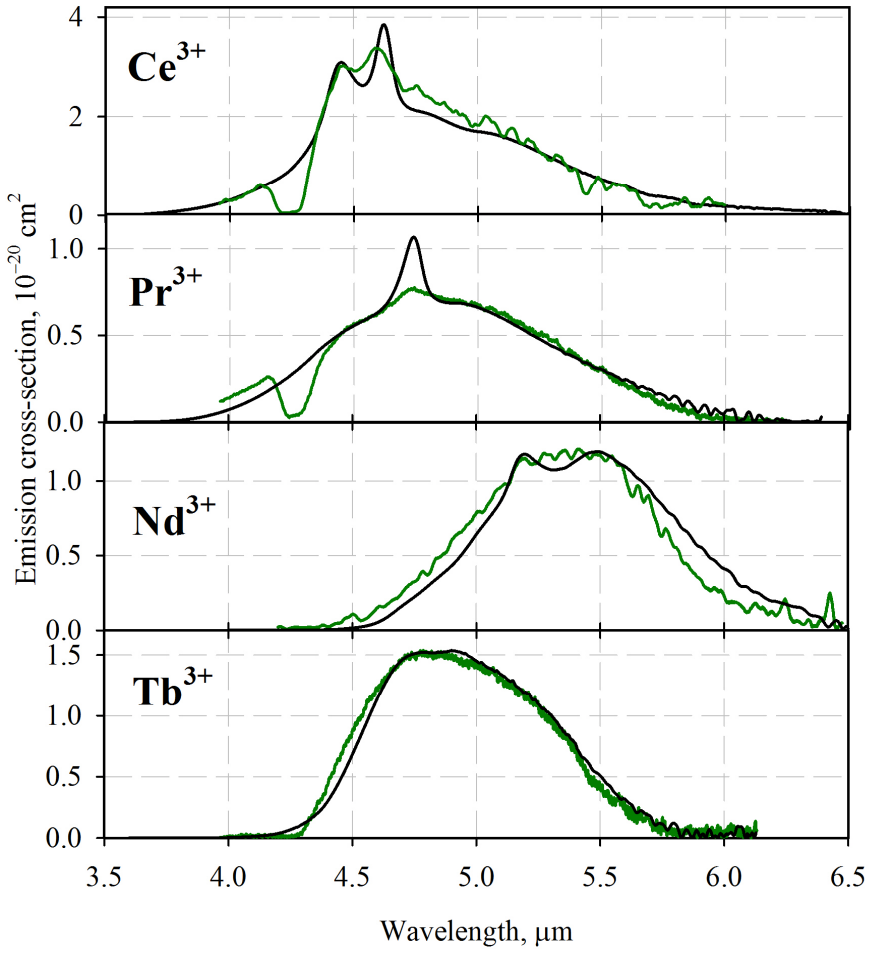

Figure 3. Stimulated emission cross-sections of rare-earth ions in $Ga_5Ge_{20}Sb_{10}Se_{65}$ glasses. Black curves–calculations based on absorption spectra. Green curves—experiment.

Table 1. First-excited-state lifetimes of rare-earth ions in selenide glass.

Active Ion	Calculated Radiative Lifetime, ms	Luminescent Lifetime (Experiment), ms
Ce^{3+}	4.72	3.7
Pr^{3+}	11.1	8.5
Nd^{3+}	20.2	10.0
Tb^{3+}	8.51	7.5

A comparison of the luminescence spectra of the four studied ions shows that the luminescence bands of Ce^{3+}, Pr^{3+} and Tb^{3+} have maxima close to 4.7 microns and overlap with each other almost completely. Notably, the Ce^{3+} cross-section is several times higher than those of the other three ions. The Nd^{3+} emission spectrum is noticeably red-shifted in comparison with the other three ions and extends beyond 6 µm. A comparison of experimental luminescent and calculated radiative lifetimes (Table 1) shows that the luminescence quantum yield in the studied selenide glasses is high (about 80%) for Ce^{3+}, Pr^{3+} and Tb^{3+} ions, and it is about 50% for the longer-wavelength transition of Nd^{3+}.

4. Pumping Schemes and Sources for the Selected Rare-Earth-Ion Transitions

Figure 4 shows the overview absorption spectra of the four selected rare-earth ions in the transmission window of selenide glasses.

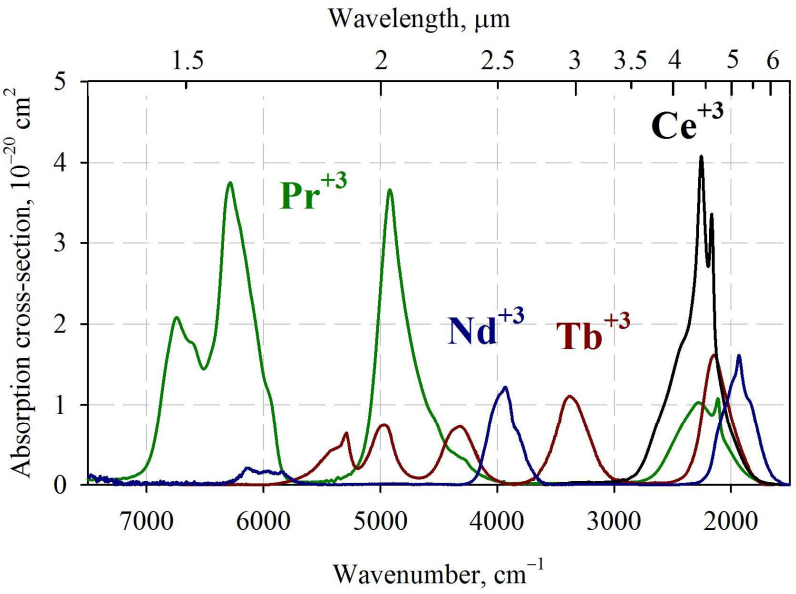

Figure 4. Absorption spectra of the selected rare-earth ions in selenide glasses.

Ce^{3+} has a single, but intense, infrared absorption band with a maximum near 4.5 µm and has to be pumped resonantly. A good candidate for the pumping source is a Fe^{2+}:ZnSe laser emitting at about 4.08 µm [38]. Another (maybe more practically convenient, but still rather expensive) class of pump sources for this active ion are the newly developed high-power quantum-cascade lasers [29].

Pr^{3+}, unlike Ce^{3+}, has several absorption bands in the 1.5–5 µm spectral interval. In principle, each of these bands can be used for optical pumping of the upper-laser-level $^3H_5$. However, as can be seen from Figure 2, the gaps on the energy scale between the high-lying, directly pumped levels and the upper laser level are comparable to the energy gap of the laser transition itself. This means that some of the high-lying levels ($^3F_3$, $^3H_6$) are also radiative, with long luminescent lifetimes. Thus, the energy of their optical excitation will be largely irradiated in the form of luminescence, without reaching the upper laser level [21]. The problem can be solved by utilizing the cross-relaxation processes taking place at high concentrations of praseodymium (about 10^{20} cm^{-3}), as was proposed in [34]. In

this case, one absorbed pump photon corresponding to a wavelength of ~1.54 microns can generate up to three Pr^{3+} ions at the upper-laser-level $^3H_5$. The efficiency of the proposed Pr^{3+} pumping method was confirmed in [39] with the example of a KPb_2Cl_5 crystal.

The energy level scheme of Nd^{3+} resembles that of Pr^{3+}. However, there is one inconvenient circumstance. There are no efficient laser sources matching the absorption bands of Nd^{3+} (at 1.7 μm and 2.5 μm). For this reason, a sensitization scheme for neodymium ions pumping in selenide glasses had to be developed.

A similar task had already been set and solved earlier in [40]. When the Nd^{3+} and Tm^{3+} co-doped KPb_2Cl_5 crystal were excited into the Tm^{3+} absorption band with a 785 nm laser diode, intensive ~5 μm luminescence from the $^4I_{11/2}$ level of Nd^{3+} took place. Unfortunately, this sensitization scheme is not applicable to selenide glasses since they are completely opaque at the mentioned pump wavelength. Therefore, we paid attention to the strong overlapping of the Tb^{3+} luminescence spectra with the absorption band of Nd^{3+} corresponding to the $^4I_{11/2}$ level and investigated the energy transfer between these ions. Our investigation [41] showed that a $Tb^{3+} \rightarrow Nd^{3+}$ energy transfer takes place indeed, but at room temperature, it is reversible and cannot provide the high Nd^{3+} $^4I_{11/2}$ population required for laser action. Nevertheless, at the liquid nitrogen temperature, the $Tb^{3+} \rightarrow Nd^{3+}$ energy transfer becomes unidirectional and suitable for Nd^{3+} mid-infrared lasing.

As for Tb^{3+} ions themselves, their energy level scheme seems to be the most convenient for ~5 μm selenide glass lasers. They have a rich absorption spectrum within the selenide glass transparency window (with peaks at 1.88 μm, 2.0 μm, 2.3 μm, 3.0 μm and 4.7 μm; see Figure 4) and can be pumped, for example, by widespread ~2 μm Tm^{3+} or ~2.9 μm Er^{3+} lasers. There is one more favorable circumstance: the energy gaps between all the high-lying levels are small. For this reason, Tb^{3+} ions in selenide glasses relax rapidly to the upper-laser-level $^7F_5$. In contrast to Pr^{3+} and Nd^{3+}, these relaxation processes do not include ion–ion interactions and take place at any doping level, which can be selected for convenience reasons.

5. Laser Experiments with Bulk Glass Samples

The first successful mid-infrared lasing experiment with rare-earth-doped chalcogenide glasses was carried out using bulk Tb^{3+}-doped selenide sample under pulsed 2.93 μm Er:YAG laser pumping [27].The pump laser emitted ~1 ms pulses at a repetition rate not exceeding 0.5 Hz. The sample (cylindrical rod Ø12 × 29 mm with polished plane-parallel ends) was placed in a resonator formed by dielectric mirrors with high reflection in the 4.5–6 μm band. The mirrors were mounted close to the laser rod ends. The experimental arrangement is shown in Figure 5.

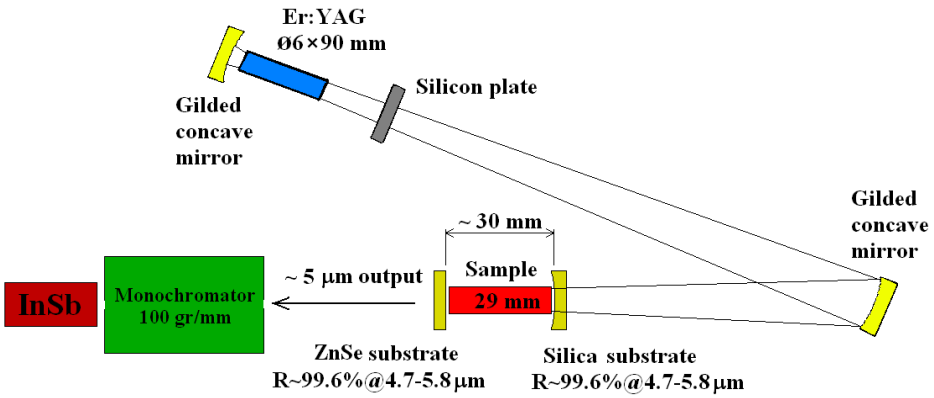

Figure 5. Laser experiment arrangement in the case of Tb-doped bulk glass.

Laser oscillations were observed at the wavelengths of 4.9–5.5 μm. This was the first evidence of laser action corresponding to the $^7F_5 \rightarrow {}^7F_6$ transition of Tb^{3+} ions and also the first case of mid-infrared lasing in a chalcogenide glass host.

A similar experiment was performed with Pr-doped glass pumped by a 1.54 μm Cr,Yb,Er: glass laser emitting ~2 ms pulses at a repetition rate of 0.2 Hz. As Figure 3 shows, the emission spectra of Tb^{3+} and Pr^{3+} are located in the same spectral band. Nevertheless, the lasing wavelengths under similar conditions turned out to be somewhat different. In the case of Pr^{3+} ions, laser action was obtained only at the long-wavelength edge of the luminescence band at 5.5–5.9 μm. This wavelength shift is most probably explained by the excited state absorption at $\lambda < 5.5$ μm from the $^3H_5$ to the $^3H_6$ level. In these first two experiments, the very occurrence of laser action was of interest. Therefore, resonator mirrors with almost 100% reflection were used, and the lasers' output energy was well below 1 mJ.

In laser experiments with Ce-doped bulk selenide glasses [38], the pump source was a 4.08 μm Fe^{2+}:ZnSe 300 μs pulsed laser which, in turn, was excited by an Er:YAG laser. Since the pump and the lasing wavelengths were close in this case, it was problematic to fabricate dielectric mirrors with high transmission at the pump wavelength combined with high reflection in the 4.5–6 μm band. For this reason, the pump beam entered the laser rod by passing the output mirror, as shown in Figure 6.

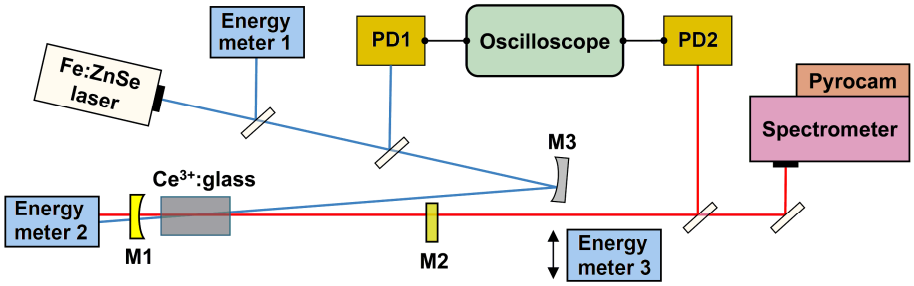

Figure 6. Laser experiment arrangement in the case of Ce-doped bulk glasses.

The high emission cross-section of Ce^{3+} ions has made it possible for us to use an outcoupling exceeding 20% and to enable practically significant output. The improved experimental conditions resulted in a maximum output energy of 43 mJ at $\lambda = 5.25$ μm, with a slope efficiency of $\eta = 25\%$ in terms of absorbed pump energy; Figure 7.

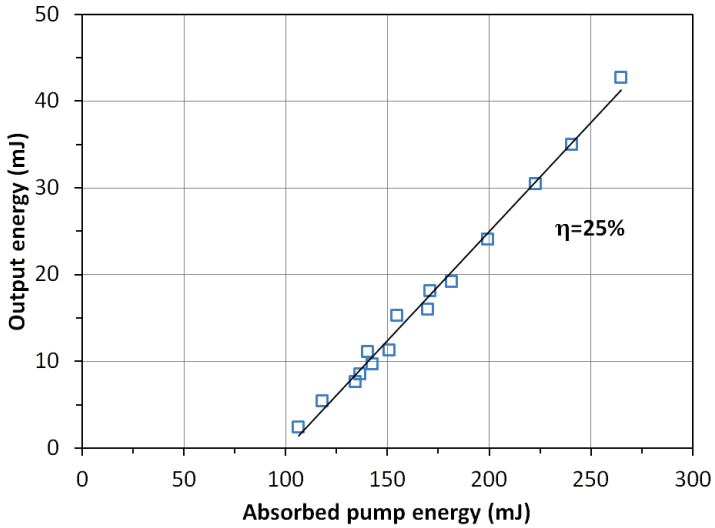

Figure 7. Output characteristic of a pulsed Ce^{3+} glass laser. The slope efficiency, η, is indicated.

For the wavelength tuning experiments, a Brewster-angle-cut CaF_2 prism was inserted into the cavity. This cavity configuration has made it possible to extend the Ce^{3+} lasing-wavelength interval to 4.6–5.6 microns; see Figure 8.

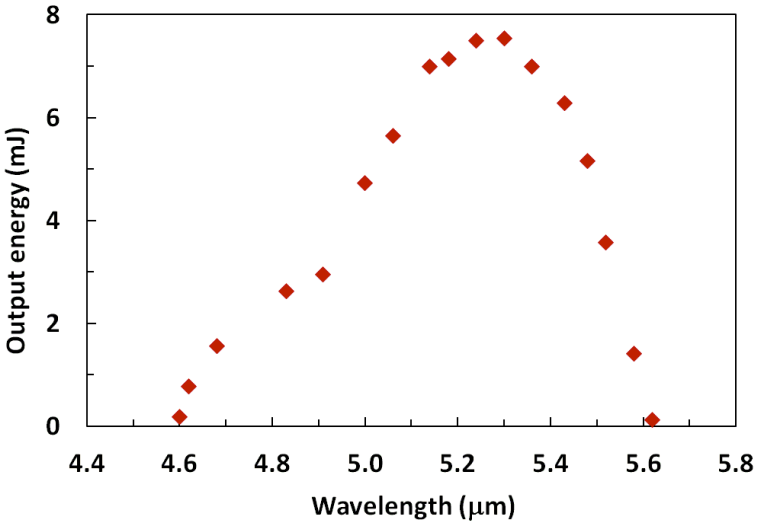

Figure 8. Tuning curve of a Ce-doped selenide glass laser at a fixed pump energy level (1.25 J).

In all the above cases, the lasing experiments were performed at room temperature, and no specific measures were taken to cool the active glass samples. In contrast, the experiment with the Tb, Nd co-doped glass was performed at liquid nitrogen temperatures [42]. As mentioned in the above section, the Nd^{3+}-doped laser glass with Tb^{3+} sensitization has to be cooled to liquid nitrogen temperature to avoid a reverse $Nd^{3+} \rightarrow Tb^{3+}$ energy transfer. The experimental arrangement for this case is shown in Figure 9.

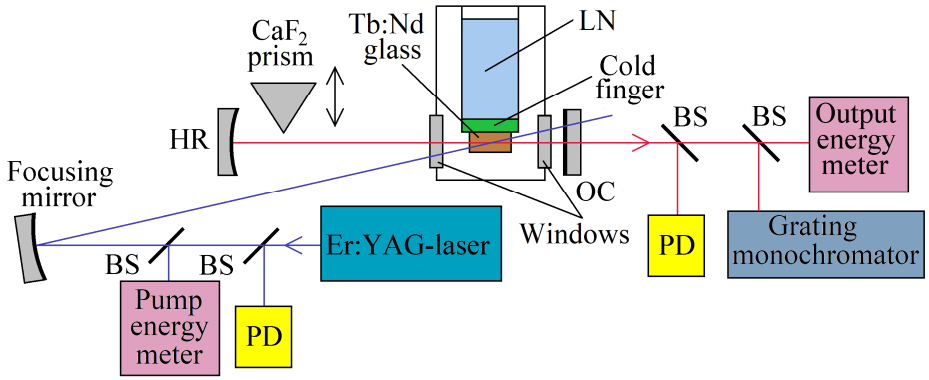

Figure 9. Laser experiment setup. HR—highly reflective mirror; OC—output coupler; BS—beam splitter; PD—photodetector.

The laser rod was mounted on a cold finger in a home-made cryostat with CaF_2 windows. The polished faces of the rod and uncoated plane-parallel CaF_2 cryostat windows were aligned perpendicular to the laser-cavity optical axis. The laser cavity was formed by a spherical aluminum mirror and a flat dielectric output coupler. For wavelength tuning experiments, a Brewster-angle-cut CaF_2 prism was inserted into the cavity. The Tb, Nd co-doped glass was pumped by a pulsed 2.94 μm Er:YAG laser into the Tb^{3+} absorption band. The pump laser operated at 0.2 Hz. The experiment confirmed the conclusion made in [41] that liquid nitrogen cooling would be required for laser action. In the absence of the intracavity prism, the lasing wavelengths were 5.7–5.85 μm, depending on the cavity Q-factor. These wavelengths lie outside the lasing spectrum of Tb^{3+} ions and can belong only to Nd^{3+} ions. Figure 10 presents the oscillograms of the pump and lasing pulses at the pump level close to the threshold (left) and well above it (right). They have a specific feature—a time delay between pump and laser pulses. This is especially evident in the plot on the left, where the laser oscillations start with a delay of 150 microseconds after the end of the pump pulse. The reason for this is the following: Tb^{3+} ions are excited

by the pump source directly, and Nd^{3+} ions are excited from Tb^{3+} ions in the process of nonradiative energy transfer within a few hundred microseconds. Thus, the observed delay also indicates that the lasing ions are Nd^{3+} and not Tb^{3+}.

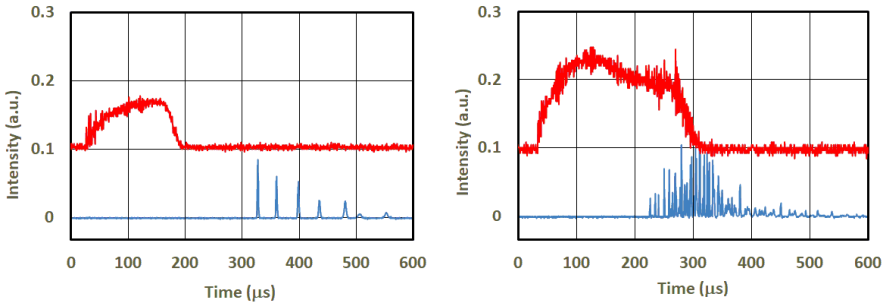

Figure 10. Oscillograms of the pump (red) and lasing (blue) pulses close to the threshold (**left**) and at the maximum pump energy (**right**).

Figure 11 shows the dependence of the laser output energy versus the pump energy incident on the laser rod for two output couplers. An output energy of up to 16 mJ was demonstrated.

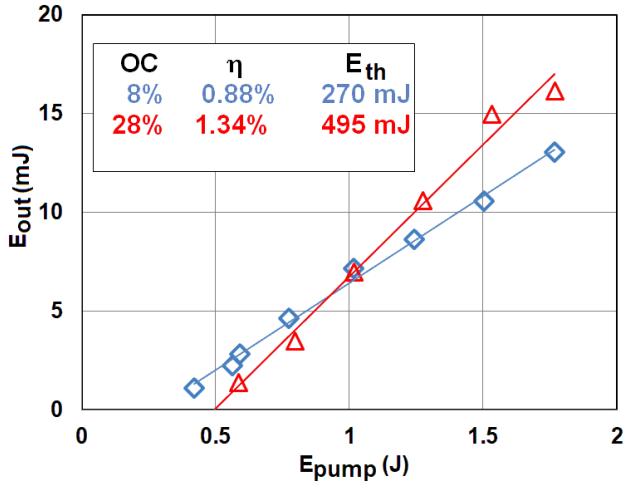

Figure 11. Output characteristics of a pulsed Nd^{3+} glass laser with two different output couplers (OC). The lasing thresholds, E_{th}, and slope efficiencies, η, are indicated.

Wavelength tuning with an intracavity CaF_2 prism widened the spectral interval of the Tb-Nd laser to 5.56~6.01 μm (Figure 12).

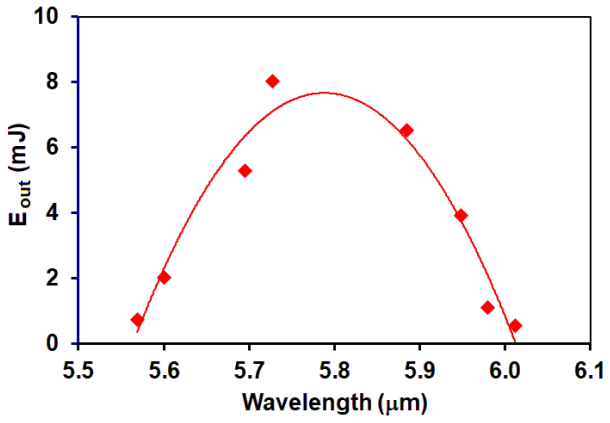

Figure 12. Tuning curve of a Nd-doped selenide glass laser.

It can be seen that the tuning range of the Nd^{3+} glass laser complements the spectral range of cerium and terbium chalcogenide glass lasers (4.5–5.6 μm) and includes the longest wavelengths for the rare-earth-doped glass lasers of today.

6. Laser Experiments with Rare-Earth-Doped Chalcogenide Glass Fibers

The experiments described in the previous section have shown that mid-infrared laser action of rare-earth-doped selenide glasses is feasible and that these lasers are capable of generating practically significant output energy. The important advantage of glasses is their ability to draw optical fibers from them. The fiber configuration easily allows a continuous operation regime, as well as achieves high gain coefficients in long active fibers. The most suitable active ions for use in fiber lasers are Tb^{3+} and Ce^{3+}. The pumping processes of these ions do not include nonradiative ion–ion interactions and, thus, there are no restrictions to the minimal active ion concentration. The number of original papers describing chalcogenide glass fiber lasers is still rather limited so far: [43] is devoted to Tb^{3+} ions and [29,44] to Ce^{3+} ions. Due to the absence of Bragg gratings in doped chalcogenide fibers developed to date in all these laser experiments, the resonators were formed by external mirrors immediately adjacent to the fiber ends or simply by the bare fiber ends, providing a ~20% Fresnel reflection.

The fiber described in [43] was manufactured by the double-crucible method. Figure 13 shows two photos of the cleaved fiber end. The core material was $Ga_5Ge_{20}Sb_{10}Se_{65}$ glass doped with 2×10^{19} cm^{-3} of Tb^{3+} ions. Undoped $Ge_{12}As_{20}Sb_5S_{63}$ sulfide glass having thermophysical properties close to those of the core material was used for the cladding. The refractive index of the cladding (2.3) turned out to be significantly lower than that of the core (2.55). The diameter of the core was 19 μm, while the diameter of the cladding was 270 μm. The cladding was protected with a fluoroplastic coating. With this geometry, the optical fiber was essentially multimode and had a numerical aperture (NA) close to unity. The fiber was mechanically strong enough to be bent to a radius of 10 cm without changing its laser characteristics. Optical losses in the fiber at λ = 1.56 μm, i.e., outside the absorption bands of terbium, were about 1.7 dB/m.

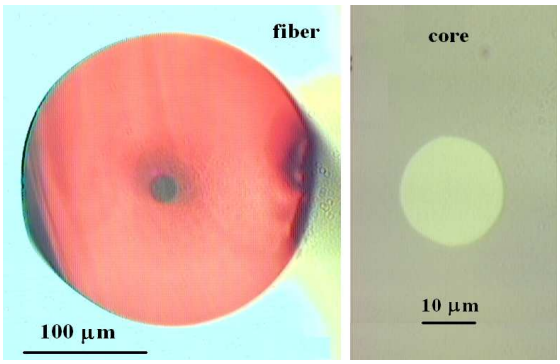

Figure 13. Photos of the cleaved fiber end and of its core.

A laser based on a 53 cm long piece of this fiber operated with an output power of up to 150 mW and a slope efficiency of 4.4%. The pump source was a continuous 1.908 μm thulium fiber laser. The wavelengths of the Tb^{3+} fiber laser lay in the spectral interval of 5.1–5.4 μm and varied slightly, depending on the Q-factor of the laser cavity and the pumping power. Typical examples of the laser output spectra are presented in Figure 14. The achieved output characteristics of this laser are shown in Figure 15.

Despite continuous pumping, the laser radiation consisted of a train of nonrelaxing spikes with a duration of about 0.5 μs. Most probably, the spiking mechanism is associated with an up-conversion process ($^7F_5 + {}^7F_5 \rightarrow {}^7F_3 + {}^7F_6$) between two excited Tb^{3+} ions. A similar effect is well known for heavily doped Er and Ho fiber lasers. Surprisingly, in most experiments, the laser output radiation had an almost Gaussian intensity distribution

over the cross-section and a divergence close to the diffraction limit, despite the essentially multimode fiber structure (Figure 16).

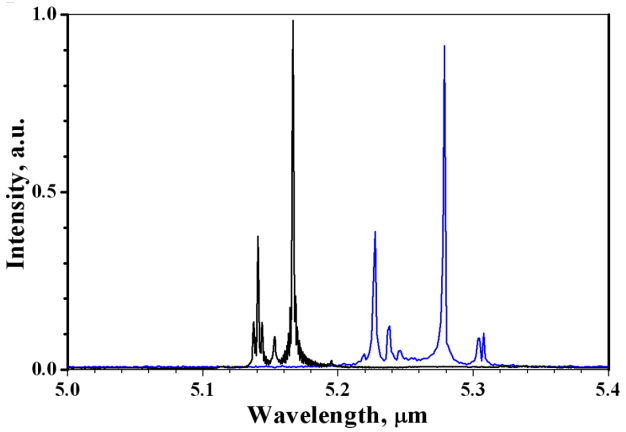

Figure 14. Two typical examples (black and blue curves) of Tb^{3+} fiber laser output spectra.

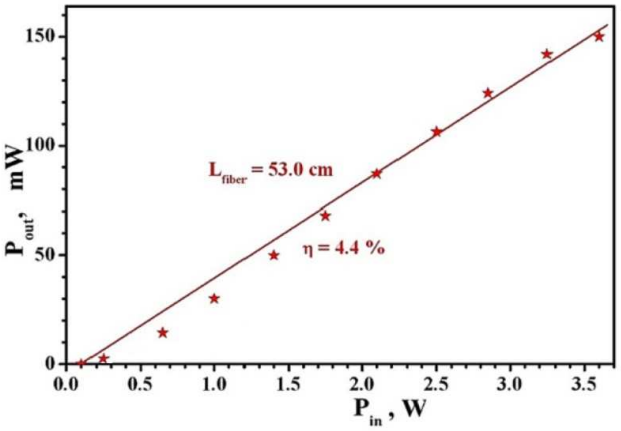

Figure 15. Dependence of the output power of the terbium fiber laser on the incident pump power.

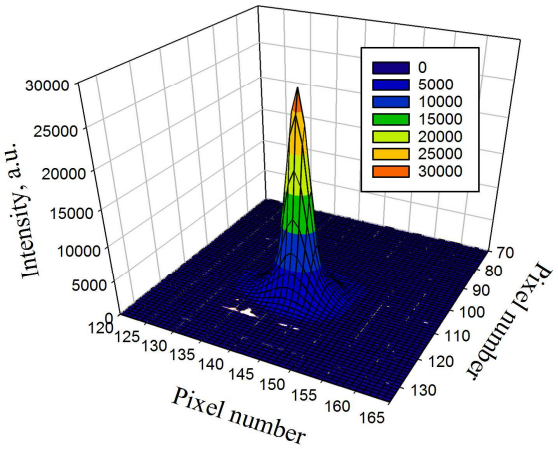

Figure 16. 3D image of the beam waist. Pixel size is 80 μm.

The paper by [29] describes Ce-doped fiber that was cladding-pumped with a 0.5 W CW quantum-cascade laser emitting at 4.15 μm. The emission spectrum showed deformation with a pump-power increase, and the threshold character of this deformation was interpreted as the startup of laser action. Spectral and temporal characteristics of a Ce^{3+}-doped chalcogenide glass fiber laser pumped by a CW Fe^{2+}:ZnSe laser were investigated

for the first time in [44]. The fiber was pumped into its core by a CW 4.16 μm Fe^{2+}:ZnSe laser having an output power of up to 70 mW. In this case, the bi-directional 4.62 μm laser radiation from the two cleaved fiber ends reached ~1 mW. At higher Q-factors (with an external mirror adjacent to one fiber end), the lasing wavelength hopped to 5.0–5.1 μm. This behavior was explained by the peculiarities of the gain spectrum, which has two characteristic maxima. It is worth noting that the CW-pumped Ce^{3+} fiber laser, unlike the Tb^{3+} laser, operated in a regular CW regime. The alleged reason for this is that the simple energy-level structure of Ce^{3+} ions does not allow for up-conversion.

7. Discussion

A comparison of mid-infrared lasing experiments with the four selected rare-earth ions in selenide glasses allows us to draw the following considerations:

Ce^{3+} and Tb^{3+} terbium ions seem to be the most convenient active ions for practical use in selenide fiber lasers. There is no need to involve complex interionic interaction processes for their pumping. Additionally, it is possible to choose their concentration from within a wide range. Cerium ions exhibit the largest emission cross-section among the four considered rare-earth ions in selenide glasses. Becoming increasingly widespread, quantum-cascade lasers are good candidates for their pumping. However, high-power quantum-cascade lasers are still expensive. As for Tb^{3+} ions, common 2 μm Tm^{3+} and 3 μm Er^{3+} lasers are suitable pumping sources for them.

The pumping of Pr^{3+} and Nd^{3+} selenide glass lasers involves complicated nonradiative interionic interaction processes. This circumstance is not an insurmountable obstacle, but it does impose some restrictions, such as the need for a high doping level and liquid nitrogen cooling.

8. Conclusions

The paper provides an overview of the latest results on 4–6 μm lasers based on rare-earth-doped selenide glasses. Pulsed laser action of Ce^{3+}, Pr^{3+}, Nd^{3+} and Tb^{3+} ions was demonstrated in bulk glass samples. Lasing of Ce^{3+}, Pr^{3+}, and Tb^{3+} ions took place at room temperature, while the Tb^{3+}-sensitized Nd^{3+} laser required liquid nitrogen cooling. The highest output parameters for bulk glasses so far (over 40 mJ of output energy, wavelength tuning in the range of 4.6–5.6 μm) were obtained with Ce^{3+}-doped glass. The highest output parameters for fiber lasers (up to 150 mW at 5.1–5.4 μm under continuous pumping) were obtained with Tb^{3+} ions. The longest lasing wavelengths for any glass laser and tunability within the 5.56–6.01 μm spectral band were obtained with Nd^{3+} ions.

9. Future Directions

The review shows that the wavelength range from 4.5 to 6 microns can be covered by rare-earth-doped selenide glass lasers in bulk and fiber configurations. It should be noted that the four laser transitions mentioned in this review do not form an exhaustive list of mid-infrared rare-earth transitions that are of interest for lasing in selenide glasses. For example, Dy^{3+} ions exhibit two promising electron transitions: a ~5 μm $^6F_{11/2} \rightarrow {}^6H_{11/2}$ transition and ~4 μm $^6H_{11/2} \rightarrow {}^6H_{13/2}$ transition. Their laser potential in selenide glasses is still to be investigated.

Two main directions for further research in this area seem to be the most promising:

The first direction is the further advancement into the infrared region. As already mentioned in Section 2, in principle, the luminescence of rare-earth ions in selenide glasses could be observed at wavelengths reaching 7–8 μm. Nevertheless, laser action at 7–8 μm transitions is hardly possible due to the low quantum yields. The situation may change after replacing the selenide glasses with telluride glasses. Unfortunately, today, there is very little literature data on the luminescent properties of rare-earth ions in telluride glasses. There is a patent [45] that contains data on a significant (about 400 microseconds) lifetime of the $^7F_4$ level corresponding to the 8 μm transition of Tb^{3+} ions in telluride glass. There are also data concerning the luminescent properties of Tb^{3+} ions in mixed selenide–telluride

compositions [33]. However, from the results of this work, it should be concluded that such mixed compositions do not provide a radical increase of 8 μm luminescence compared with selenide glasses.

The second area of research that seems promising is the fabrication of all-fiber lasers. The problem here is the undeveloped element base for chalcogenide glass fibers; Bragg fiber gratings in particular. Bragg gratings should make it possible to bring chalcogenide fiber lasers from the experimental laboratory level to the level of serviceable devices. A review [46] describes the inscription of Bragg gratings into arsenic sulfide and selenide glass fibers by laser radiation, whose wavelengths fall on the short-wave boundary of the transparency region of the glasses used. Unfortunately, two-component arsenic chalcogenide glasses do not allow rare-earth doping, and there are currently no literature data on Bragg grating inscription into germanium-based chalcogenide glass fibers that allow rare-earth doping. Thus, to create all-fiber lasers based on chalcogenide fibers doped with rare earths, it will be necessary to either develop a technology for Bragg grating inscription directly in doped fibers or to work out a technique for the splicing of active and passive chalcogenide fibers of substantially different compositions.

Author Contributions: Conceptualization, B.D., B.G., V.P., M.S., S.S. and A.V.; writing—original draft preparation, S.S.; writing—review and editing, B.D., P.F., M.F., B.G., V.P., M.S., S.S. and A.V.; visualization, V.K.; supervision, B.D. All authors have read and agreed to the published version of the manuscript.

Funding: This research received no external funding.

Institutional Review Board Statement: Not applicable.

Informed Consent Statement: Not applicable.

Data Availability Statement: No new data were created or analyzed in this study. Data sharing is not applicable to this article.

Conflicts of Interest: The authors declare no conflict of interest.

References

1. Ebrahim-Zadeh, M.; Sorokina, I.T. *Mid-Infrared Coherent Sources and Applications*; Springer: Dordrecht, The Netherlands, 2008.
2. Pollock, C.R.; Pinto, J.F.; Georgiou, E. Recent progress in color center lasers. *Appl. Phys. B* **1989**, *48*, 287–292. [CrossRef]
3. Vitiello, M.S.; Scalari, G.; Williams, B.; De Natale, P. Quantum cascade lasers: 20 years of challenges. *Opt. Express* **2015**, *23*, 5167–5182. [CrossRef] [PubMed]
4. Mirov, S.B.; Moskalev, I.S.; Vasilyev, S.; Smolski, V.; Fedorov, V.V.; Martyshkin, D.; Peppers, J.; Mirov, M.; Dergachev, A.; Gapontsev, V. Frontiers of Mid-IR Lasers Based on Transition Metal Doped Chalcogenides. *IEEE J. Sel. Top. Quantum Electron.* **2018**, *24*, 1601829. [CrossRef]
5. Evans, J.W.; Dolasinski, B.D.; Harris, T.R.; Cleary, J.W.; Berry, P.A. Demonstration and power scaling of an Fe:CdMnTe laser at 52 microns. *Opt. Mater. Express* **2017**, *7*, 860. [CrossRef]
6. Doroshenko, M.E.; Jelínková, H.; Jelínek, M.; Šulc, J.; Vyhlídal, D.; Kovalenko, N.O.; Terzin, I.S. Room temperature Fe^{2+}: $Cd_{1-x}Mn_xTe$ laser generating at 5.4–6 μm. *Opt. Lett.* **2018**, *43*, 5058. [CrossRef]
7. Pushkin, A.; Migal, E.; Suleimanova, D.; Mareev, E.; Potemkin, F. High-Power Solid-State Near- and Mid-IR Ultrafast Laser Sources for Strong-Field Science. *Photonics* **2022**, *9*, 90. [CrossRef]
8. Antonov, V.A.; Firsov, K.N.; Gavrishchuk, E.M.; Ikonnikov, V.B.; Kononov, I.G.; Kurashkin, S.V.; Podlesnykh, S.V.; Savin, D.V.; Zhavoronkov, N.V. DF laser pumped single-crystal Fe:CdTe laser operating at room temperature. *Laser Phys. Lett.* **2023**, *20*, 045802. [CrossRef]
9. Bowman, S.; Ganem, J.; Feldman, B.; Kueny, A. Infrared laser characteristics of praseodymium-doped lanthanum trichloride. *IEEE J. Quantum Electron.* **1994**, *30*, 2925. [CrossRef]
10. Bowman, S.; Searles, S.K.; Jenkins, N.W.; Qadri, S.B.; Skelton, E.F.; Ganem, J. Diode pumped room temperature 4.6 μm erbium laser. In *Advanced Solid State Lasers*; Optical Society of America; Optica Publishing Group: Washington, DC, USA, 2001. [CrossRef]
11. Jelinkova, H.; Sulc, J.; Jelínek, M.; Nemec, M.; Fibrich, M.; Doroshenko, M.E.; Osiko, V.V.; Badikov, V.V.; Badikov, D.V. Mid-IR radiation generated by Dy: $PbGa_2S_4$ laser. In *Advanced Solid State Lasers*; OSA Technical Digest; Optica Publishing Group: Washington, DC, USA, 2014; paper ATu2A.12. [CrossRef]
12. Okhrimchuk, A.G.; Butvina, L.N.; Dianov, E.M.; Shestakova, I.A.; Lichkova, N.V.; Zagorodnev, V.N.; Shestakov, A.V. Optical spectroscopy of the $RbPb_2Cl_5$: Dy^{3+} laser crystal and oscillation at 5.5 μm at room temperature. *J. Opt. Soc. Am. B* **2007**, *24*, 2690. [CrossRef]

13. Maes, F.; Fortin, V.; Poulain, S.; Poulain, M.; Carrée, J.-Y.; Bernier, M.; Vallée, R. Room-temperature fiber laser at 3.92 μm. *Optica* **2018**, *5*, 761–764. [CrossRef]
14. Bufetov, I.A.; Kosolapov, A.F.; Pryamikov, A.D.; Gladyshev, A.V.; Kolyadin, A.N.; Krylov, A.A.; Yatsenko, Y.P.; Biriukov, A.S. Revolver Hollow Core Optical Fibers. *Fibers* **2018**, *6*, 39. [CrossRef]
15. Zhou, Z.; Huang, W.; Chui, Y.; Li, H.; Pei, W.; Li, X.; Li, Z.; Wang, M.; Wang, Z. 3.1 W mid-infrared fiber laser at 4.16μm based on HBr-filled hollow-core silica fibers. *Opt. Lett.* **2022**, *47*, 5785–5788. [CrossRef] [PubMed]
16. Seddon, A.B.; Sojka, L.; Furniss, D.; Tang, Z.; Crane, R.; Nunes, J.; Phang, S.; Barney, E.; Farries, M.C.; Benson, T.M.; et al. Mid-infrared sources, based on chalcogenide glass fibres, for biomedical diagnostics. In *Optical Fibers and Sensors for Medical Diagnostics, Treatment and Environmental Applications XXI*; SPIE: Bellingham, WA, USA, 2021; Volume 11635, p. 1163503. [CrossRef]
17. Shaw, L.; Cole, B.; Thielen, P.; Sanghera, J.; Aggarwal, I. Mid-wave IR and long-wave IR laser potential of rare-earth doped chalcogenide glass fiber. *IEEE J. Quantum Electron.* **2001**, *37*, 1127–1137. [CrossRef]
18. Jackson, S.D.; Jain, R.K. Fiber-based sources of coherent MIR radiation: Key advances and future prospects. *Opt. Express* **2020**, *28*, 30964–31019. [CrossRef] [PubMed]
19. Seddon, A.B.; Sójka, Ł.; Chen, M.; Tang, Z.; Furniss, D.; Barney, E.; Sakr, H.; Jayasuriya, D.; Parnell, H.; Butterworth, J.; et al. Breaking through the wavelength barrier: The state-of-play on rare-earth ion, mid-infrared fiber lasers for the 4–10 μm wavelength region. In *Mid-Infrared Fiber Photonics*; Jackson, S., Vallee, R., Bernier, M., Eds.; Elsevier: Amsterdam, The Netherlands, 2021; pp. 401–502. [CrossRef]
20. Moizan, V.; Nazabal, V.; Troles, J.; Houizot, P.; Adam, J.-L.; Doualan, J.-L.; Moncorgé, R.; Smektala, F.; Gadret, G.; Pitois, S.; et al. Er^{3+}-doped GeGaSbS glasses for mid-IR fibre laser application: Synthesis and rare earth spectroscopy. *Opt. Mater.* **2008**, *31*, 39–46. [CrossRef]
21. Sójka, Ł.; Tang, Z.; Zhu, H.; Bereś-Pawlik, E.; Furniss, D.; Seddon, A.B.; Benson, T.M.; Sujecki, S. Study of mid-infrared laser action in chalcogenide rare earth doped glass with Dy^{3+}, Pr^{3+} and Tb^{3+}. *Opt. Mater. Express* **2012**, *2*, 1632–1640. [CrossRef]
22. Seddon, A.B.; Tang, Z.; Furniss, D.; Sujecki, S.; Benson, T.M. Progress in rare-earth-doped mid-infrared fiber lasers. *Opt. Express* **2010**, *18*, 26704. [CrossRef] [PubMed]
23. Heo, J.; Chung, W.J. Rare-earth-doped chalcogenide glass for lasers and amplifiers. In *Chalcogenide Glases*; Adam, J.-L., Zhang, X., Eds.; Woodhead Publishing: Cambridge, UK, 2014; Chapter 11; pp. 347–380. [CrossRef]
24. Schweizer, T.; Hewak, D.; Payne, D.; Jensen, T.; Huber, G. Rare-earth doped chalcogenide glass laser. *Electron. Lett.* **1996**, *32*, 666–667. [CrossRef]
25. Sukhanov, M.V.; Velmuzhov, A.P.; Otopkova, P.A.; Ketkova, L.A.; Evdokimov, I.I.; Kurganova, A.E.; Plotnichenko, V.G.; Shiryaev, V.S. Rare earth elements as a source of impurities in doped chalcogenide glasses. *J. Non-Cryst. Solids* **2022**, *593*, 121793. [CrossRef]
26. Shen, M.; Furniss, D.; Farries, M.; Jayasuriya, D.; Tang, Z.; Sojka, L.; Sujecki, S.; Benson, T.M.; Seddon, A.B. Experimental observation of gain in a resonantly pumped Pr^{3+}-doped chalcogenide glass mid-infrared fibre amplifier notwithstanding the signal excited-state absorption. *Sci. Rep.* **2019**, *9*, 11426. [CrossRef]
27. Churbanov, M.F.; Denker, B.I.; Galagan, B.I.; Koltashev, V.V.; Plotnichenko, V.G.; Sverchkov, S.E.; Sukhanov, M.V.; Velmuzhov, A.P. First demonstration of ~5 μm laser action in terbium doped selenide glass. *Appl. Phys. B* **2020**, *126*, 117. [CrossRef]
28. Tang, Z.; Sojka, L.; Furniss, D.; Nunes, J.; Sakr, H.; Barney, E.; Sujecki, S.; Benson, T.M.; Seddon, A.B. Comparative study of praseodymium additives in active selenide chalcogenide optical fibers. *Opt. Mater. Express* **2018**, *8*, 3910–3926. [CrossRef]
29. Nunes, J.J.; Sójka, Ł.; Crane, R.W.; Furniss, D.; Tang, Z.Q.; Mabwa, D.; Xiao, B.; Benson, T.M.; Farries, M.; Kalfagiannis, N.; et al. Room temperature mid-infrared fiber lasing beyond 5 μm in chalcogenide glass small-core step index fiber. *Opt. Lett.* **2021**, *46*, 3504–3507. [CrossRef] [PubMed]
30. Sukhanov, M.; Velmuzhov, A.; Ketkova, L.; Otopkova, P.; Evdokimov, I.; Kurganova, A.; Shiryaev, V.; Denker, B.; Galagan, B.; Koltashev, V.; et al. Method for preparing high-purity REE-doped chalcogenide glasses for bulk and fiber lasers operating at ~5μm region. *J. Non-Cryst. Solids* **2023**, *608*, 122256. [CrossRef]
31. Starecki, F.; Brand, A.; Abdellaoui, N.; Boussard-Pledel, C.; Bureau, B.; Nazabal, V. 7 to 8 μm emission from Sm^{3+} doped selenide fibers. *Opt. Express* **2018**, *26*, 26462–26469. [CrossRef]
32. Starecki, F.; Abdellaoui, N.; Braud, A.; Doualan, J.-L.; Boussard-Pledel, C.; Bureau, B.; Camy, P.; Nazabal, V. 8 μm luminescence from a Tb^{3+} GaGeSbSe fiber. *Opt. Lett.* **2018**, *43*, 1211–1244. [CrossRef] [PubMed]
33. Abdellaoui, N.; Starecki, F.; Boussard-Pledel, C.; Shpotyuk, Y.; Doualan, J.-L.; Braud, A.; Baudet, E.; Nemec, P.; Chevire, F.; Dussauze, M.; et al. Tb^{3+}doped $Ga_5Ge_{20}Sb_{10}Se_{65-x}Te_x$ (x = 0–37.5) chalcogenide glasses and fibers for MWIR and LWIR emissions. *Opt. Mater. Express* **2018**, *8*, 2887–2900. [CrossRef]
34. Churbanov, M.F.; Denker, B.I.; Galagan, B.I.; Koltashev, V.V.; Plotnichenko, V.G.; Sverchkov, S.E.; Sukhanov, M.V.; Velmuzhov, A.P. Peculiarities of 1.6–7.5 μm Pr^{3+}luminescence in $Ge_{36}Ga_5Se_{59}$ glass. *Opt. Mat. Express* **2019**, *9*, 4154–4164. [CrossRef]
35. Crane, R.W.; Sójka, Ł.; Furniss, D.; Nunes, J.; Barney, E.; Farries, M.C.; Benson, T.M.; Sujecki, S.; Seddon, A.B. Experimental photoluminescence and lifetimes at wavelengths including beyond 7 microns in Sm^{3+}-doped selenide-chalcogenide glass fibers. *Opt. Express* **2020**, *28*, 12373–12384. [CrossRef]
36. Sojka, L.; Tang, Z.; Jayasuriya, D.; Shen, M.; Nunes, J.; Furniss, D.; Farries, M.; Benson, T.; Seddon, A.; Sujecki, S. Milliwatt-Level Spontaneous Emission Across the 3.5–8 μm Spectral Region from Pr^{3+} Doped Selenide Chalcogenide Fiber Pumped with a Laser Diode. *Appl. Sci.* **2020**, *10*, 539. [CrossRef]

37. Churbanov, M.F.; Denker, B.I.; Galagan, B.I.; Koltashev, V.V.; Plotnichenko, V.G.; Sukhanov, M.V.; Sverchkov, S.E.; Velmuzhov, A.P. Comparison of 4.5-6 μm luminescent and lasing properties of rare earth dopants in chalcogenide glasses. *J. Lumin.* **2022**, *245*, 118756. [CrossRef]
38. Denker, B.I.; Galagan, B.I.; Sverchkov, S.E.; Koltashev, V.V.; Plotnichenko, V.G.; Sukhanov, M.V.; Velmuzhov, A.P.; Frolov, M.P.; Korostelin, Y.V.; Kozlovsky, V.I.; et al. Resonantly pumped Ce^{3+} mid-infrared lasing in selenide glass. *Opt. Lett.* **2021**, *46*, 4002–4004. [CrossRef] [PubMed]
39. Merkle, L.; Fleischman, Z.; Brown, E.; Allen, J.; Hommerich, U.; Dubinskii, M. Enhanced mid-infrared emission of Pr^{3+}ions in solids through a "3-for-1" excitation process—Quantified. *Opt. Express* **2021**, *29*, 39001. [CrossRef] [PubMed]
40. Bluiett, A.G.; Condon, N.J.; O'Connor, S.; Bowman, S.R.; Logie, M.; Ganem, J. Thulium-sensitized neodymium in KPb_2Cl_5 for mid-infrared laser development. *J. Opt. Soc. Am. B* **2005**, *22*, 2250–2256. [CrossRef]
41. Denker, B.I.; Frolov, M.P.; Galagan, B.I.; Koltashev, V.V.; Korostelin, Y.V.; Plotnichenko, V.G.; Sukhanov, M.V.; Sverchkov, S.E.; Velmuzhov, A.P. Sensitization of 5–6 μm Nd^{3+} luminescence in selenide glass by Tb^{3+} ions. *J. Lumin.* **2023**, *263*, 120056. [CrossRef]
42. Denker, B.I.; Frolov, M.P.; Galagan, B.I.; Koltashev, V.V.; Plotnichenko, V.G.; Sverchkov, S.E.; Velmuzhov, A.P. Application of non-radiative energy transfer from Tb^{3+} to Nd^{3+} for pumping a 6 μm solid-state laser. *J. Lumin.* **2023**, *266*, 120288. [CrossRef]
43. Koltashev, V.V.; Denker, B.I.; Galagan, B.I.; Snopatin, G.E.; Sukhanov, M.V.; Sverchkov, S.E.; Velmuzhov, A.P.; Plotnichenko, V.G. 150 mW Tb^{3+} doped chalcogenide glass fiber laser emitting at $\lambda > 5$ μm. *Opt. Laser Technol.* **2023**, *161*, 109233. [CrossRef]
44. Koltashev, V.V.; Frolov, M.P.; O Leonov, S.; E Sverchkov, S.; I Galagan, B.; Korostelin, Y.V.; Skasyrsky, Y.K.; E Snopatin, G.; Sukhanov, M.V.; Velmuzhov, A.P.; et al. Characteristics of a CW~5 μm Ce^{3+}-doped chalcogenide glass fiber laser. *Laser Phys. Lett.* **2023**, *20*, 095801. [CrossRef]
45. Harbison, B.; Sanghera, J.; Shaw, B.; Aggarwal, I. Rare Earth Soluble Telluride Glass. U.S. Patent 6,015,765, 18 January 2000.
46. Cai, D.; Xie, Y.; Guo, X.; Wang, P.; Tong, L. Chalcogenide Glass Microfibers for Mid-Infrared Optics. *Photonics* **2021**, *8*, 497. [CrossRef]